



# Post-drill geophysical characterization of two deep-water wells of Cauvery Basin, East Coast of India

Minakshi Mishra<sup>1</sup> · Atul Kumar Patidar<sup>2</sup>

Received: 29 June 2021 / Accepted: 8 July 2022 / Published online: 26 July 2022  
© The Author(s) 2022

## Abstract

The depth of the reservoir causes an increase in the degree of uncertainty in the prediction of reservoir quality. High frequency is suppressed with depth because Earth functions as a low-pass filter. The seismic amplitudes observed at various interfaces are influenced by spherical divergence, transmission losses, mode conversions, and inter-bed multiples. Seismic data have numerous essential components that must be thoroughly examined during hydrocarbon prospect identification and maturation, including post-critical reflections, events coherency (in near and far offsets), mode conversion, and interbed multiples. Seismic amplitudes are typically derived from 2D/3D seismic data and utilized directly or indirectly for reservoir interpretation and better prediction of subtle geological and geophysical information. To accurately depict subsurface geological features, stratigraphic architecture, and reservoir facies, it should be used in conjunction with the existing paleoenvironment data. When employed alone, the subsurface geophysical data may lead to erroneous interpretation of subsurface lithologies and inaccurate reservoir property predictions. Understanding these factors could help interpreters make better use of seismic data while maturing and de-risking the prospectivity. This study examines the post-drill geophysical characterization of two exploratory wells that were drilled in the deep-water area of the Cauvery Basin, East Coast of India. Analysis and correlation with a discovery well is done to understand the sediment depositional heterogeneity and corresponding seismic amplitude response, primarily for the cemented reservoir (dry well). To discover prospects and subsequently de-risk the existing prospect inventory, a dashboard checklist for in-depth study of seismic and well data has been developed. The top-down geophysical analytical approach that has been presented will aid in defining reservoir characteristics generally, estimating deliverability, and subsequently raising the geological probabilities and chance of success (COS) of any exploration project. The findings of this study allow critical analysis of seismic data to distinguish between softer/slower/possibly better reservoir rocks and hard/fast/tight rocks.

**Keywords** Amplitude variation with offset (AVO) · PSDM gathers · Critical reflections · Internal multiples · Seismic amplitudes · Cauvery basin · Deep-water · Turbidite channel-lobe

## Introduction

The deep-water hydrocarbon potential of East Indian passive margin sedimentary basins has been well-established in the last two decades (Qin et al. 2017; Zhang et al. 2019). The Krishna–Godavari (KG) and Cauvery Basin are considered Category-I basins having several producing fields and huge

unlocked potential of hydrocarbon presence in their deep-water areas. The current study area falls in the northern part of the Cauvery Basin (Ariyalur–Pondicherry sub-basin), located in the Tamil Nadu state, along the Palk Strait and Coromandel coast. Sedimentary basins of the eastern periphery of the Indian peninsular are formed as a result of the Indian–Antarctic break-up during the Late Jurassic–Early Cretaceous period (Sastri et al. 1981; Watkinson et al. 2007; Lal et al. 2009; Nagendra and Nallapa Reddy 2017). The NE–SW trending normal faults originated during the initial rift phase of the Cauvery Basin. The structural trend was similar to the other two rift basins located towards the north. This rifting phase resulted in the formation of NE striking series of horst-graben structures (Fig. 1), which is indicative

✉ Atul Kumar Patidar  
atulpatidar@gmail.com; apatidar@ddn.upes.ac.in

<sup>1</sup> CGI, Bangalore 560037, India

<sup>2</sup> Department of Petroleum Engineering and Earth Sciences, University of Petroleum and Energy Studies, Dehradun 248007, Uttarakhand, India

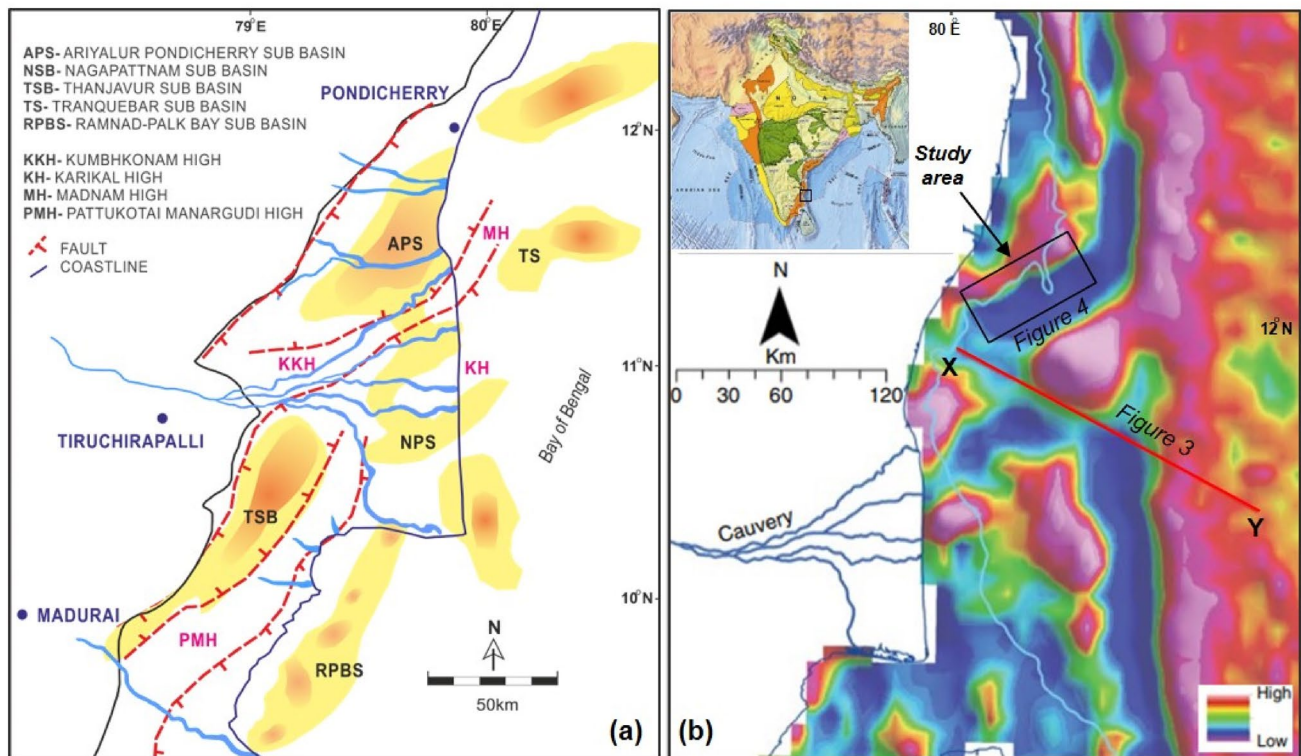


**Fig. 1** **a** Map showing major tectonic elements of the Cauvery Basin and their offshore extension. **b** Bouguer gravity anomaly map of the Cauvery Basin confirms the extension of regional tectonic elements into the deeper water. The image is reproduced with permission

(Misra and Dasgupta 2018). The shelf-slope boundary is shown by a light blue line. An NW–SE trending red line (X–Y) is location of the regional seismic section shown in Fig. 3

of extension and crustal stretching (Narasimha Chari et al. 1995; Chand and Subrahmanyam 2001; Twinkle et al. 2016; Qin et al. 2017). These parallel trending subsurface highs are separating depressions from one another and extend into the offshore area (Fig. 1). The oblique-slip separation between Antarctica and the Eastern margin of India took place along the Coromondal transform margin resulting in oblique trending horse-tail structures (Nemčok et al. 2013, 2016; Dasgupta 2019).

During the postrift thermal subsidence (Late Cretaceous), regional unconformities were formed in almost all the eastern margin basins of India (Qin et al. 2017). After the Late Cretaceous period, Cauvery Basin started growing in a shelf-slope setting and subsequently matured as a passive margin basin (Sastri et al. 1973; Chand and Subrahmanyam 2001). The deep-water region of Cauvery-Palar basin behaved as a single depression center post Late Cretaceous with sediment input from the west by Cauvery, Palar and other subsidiary rivers. An overall basinward prograding shelf-slope system was developed, mainly from mid-Miocene and the entire depositional system had prograded eastward into deep-water areas (Biswas et al. 1993; Twinkle et al. 2016; Chakraborty and Sarkar 2018). The Cauvery Basin can be divided into the following sub-basins, (i) The Ariyalur–Pondicherry

sub-basin, (ii) Nagapattinam sub-basin, (iii) Tanjore sub-basin, (iv) Tranquebar sub-basin, (v) Ramnad-Palk bay sub-basin, and (vi) Gulf of Mannar sub-basin. The basement high trends that separate these sub basins are: Kumbakonam–Madanam–Portonovo high, Pattukottai–Mannargudi–Vedaranyam–Karaikal high, and Mandapam–Delft high (Fig. 1).

The oil and gas exploration activities have resulted in economically viable hydrocarbon discoveries from both onshore and offshore regions of the Cauvery basin in the recent past (Rigzone 2007, 2013; Lasitha et al. 2019). A large amount of geological and geophysical data acquired by various Exploration and Production (E&P) companies signifies the deep-water hydrocarbon potential of this basin ([www.dghindia.gov.in](http://www.dghindia.gov.in)). The accumulation of hydrocarbon has been proven in the fractured basement and clastic sediments (mainly deep-water turbidite sandstone) of the Albian-Cretaceous age by public and private E&P companies (Qin et al. 2017; Zhang et al. 2019). The present study attempts a comprehensive analysis of the post-drill geophysical data of two exploratory wells drilled by Reliance Industries Limited (E&P) in the deep-water Cauvery Basin. A sincere attempt has been made to develop a workflow for detailed geophysical analysis using available seismic and well data. This workflow will

provide an analog for the identification and prediction of reservoir properties of deep-water siliciclastic deposits with higher accuracy and therefore lead to de-risking of the reservoir quality and deliverability. A comprehensive post-drilled analysis of the two exploratory wells drilled in a similar depositional setup in the deep-water (~ 1200 m water depth) of the Cauvery Basin (Ariyalur–Pondicherry sub-basin) was systematically carried out and presented in this paper. The first well (well A) resulted in a gas discovery, while the second well (well B) encountered diagenetically altered tight sands and was declared as a dry well. A methodical post-drill analysis was carried out to understand the geological differences encountered in both the wells and to list down the geophysical uncertainties that were missed before drilling. The reservoirs discussed in the current study lie at ~ 3200 m depth and had compressional velocities higher than the background shales. Therefore, the reflections generated at far offsets in the high impedance sands and their interference with amplitude versus offset (AVO) effects were critically examined. Various seismic attributes were also used in conjunction with detailed geophysical analysis to understand the reservoir heterogeneity and reasons for failure. Bright positive or negative seismic amplitudes on zero-phase data (depending on the polarity of seismic data) are commonly indicative of hydrocarbon-filled sands at shallower depths. But for the deeper and older rocks, a minor acoustic impedance (AI) difference is observed between hydrocarbon-bearing reservoir rocks and surrounding shaly rocks (Hanafy et al. 2018; Mishra and Singh 2019; Fawad et al. 2020). A minor difference in acoustic impedance is not strong enough to produce diagnostic seismic amplitude on stacked data. AVO analysis on CMP gathers is then used for the identification of sandy intervals and distinguishing the properties of pore fluid (Mishra and Singh 2019). In the current paper, Sect. 4 systematically explains the pre-drill prediction of both the wells, post-drill analysis of gathers, critical-angle reflection analysis, synthetic seismogram correlation and AVO modeling outcomes. A detailed geophysical dashboard was prepared based on the comparative analysis of available subsurface data of both the drilled wells and discussed in Sect. 5.

## Generalized stratigraphy of the basin

The Cauvery Basin covers ~ 50,000 sq km of the area from the onshore to offshore (up to 2000 m bathymetry) and preserves 3–6 km of sediment thickness. The geological history of this basin began with the rejuvenation of rifting during the Late Jurassic–Early Cretaceous period between the East Indian margin and Antarctica along the dextral transfer Coromondal fault zone (Sastri et al. 1981; Biswas et al. 1993; Nemčok et al. 2013; Mazumder et al. 2019).

This significant tectonic event resulted in the formation of synrift structures in the present-day deep-water Cauvery-Palar Basins (Chakraborty and Sarkar 2018). The Ramnad and the Mannar sub-basin appear to have come into existence in the earliest stage of basin formation as the non-marine sedimentary rocks (Shivganga and Tehrani formations) of the Gondwana age are deposited in these regions (Nagendra et al. 2018). On the other side, the northern sub-basins such as Tranquebar, Tanjore, Nagapattinam and Ariyalur–Pondicherry (Fig. 1) went through the initial stage of formation as a result of shear coupling and rifting, which resulted in basin deepening and hence led to initial marine incursion (Sastri et al. 1973; Chetty and Rao 2006; Mazumder et al. 2019). The tectonically controlled Cauvery Basin preserves a complete sequence of Late Jurassic to Early Cretaceous sediments, which continued till the end of the Tertiary (Fig. 2) (Muthuvairvasamy et al. 2003; Nagendra et al. 2013). For a better understanding of readers, a generalized stratigraphy of the Cauvery Basin (modified after, <https://www.ndrdgh.gov.in/NDR/>) and a description of syn- and postrift tectono-geological evaluation of the basin are shown in Fig. 2. A brief explanation is given in subsequent subsections.

### Synrift stratigraphy (Late Jurassic to Early Cretaceous)

Early synrift and basement formations are drilled in various offshore wells of the Cauvery-Palar Basins showing an active petroleum system from onshore to the deep-water area (Zhang et al. 2019). The outcrop exposures and onshore drilling data of the basin reveal that the Pre-Cambrian cratonic rocks are comprised of Granites, Gneisses, and Charnockite. Initial synrift and early postrift sediments ranging between late Jurassic to early Cretaceous age are clubbed together and named as Andimadam Formation (Janardhanan et al. 2013; Saravanan and Johny 2018; Chakraborty and Sarkar 2018), which is mainly comprised of feldspathic, gritty and kaolinitic sediments. The uppermost Andimadam Formation is dated as of the Albian age and represented by marine sediments (Fig. 2). In the deep-water offshore region, synrift sediments were drilled in wells CYPRIID7-A1, PRIIID8, CYIID5-M1, and CYIID5-S1 by Reliance industries limited (Rigzone 2007, 2013; Bastia et al. 2010; Mishra and Singh 2019; Zhang et al. 2019). The synrift sediments drilled in the above-mentioned wells were comprised of feldspathic sandstone, and siltstone along with discrete high TOC carbonaceous shale deposited in shallow marine to the lagoonal environment.

### Postrift stratigraphy (Late Cretaceous and above)

The postrift Cretaceous sag phase is mainly comprised of Aptian-Albian sediments deposited in the deep marine

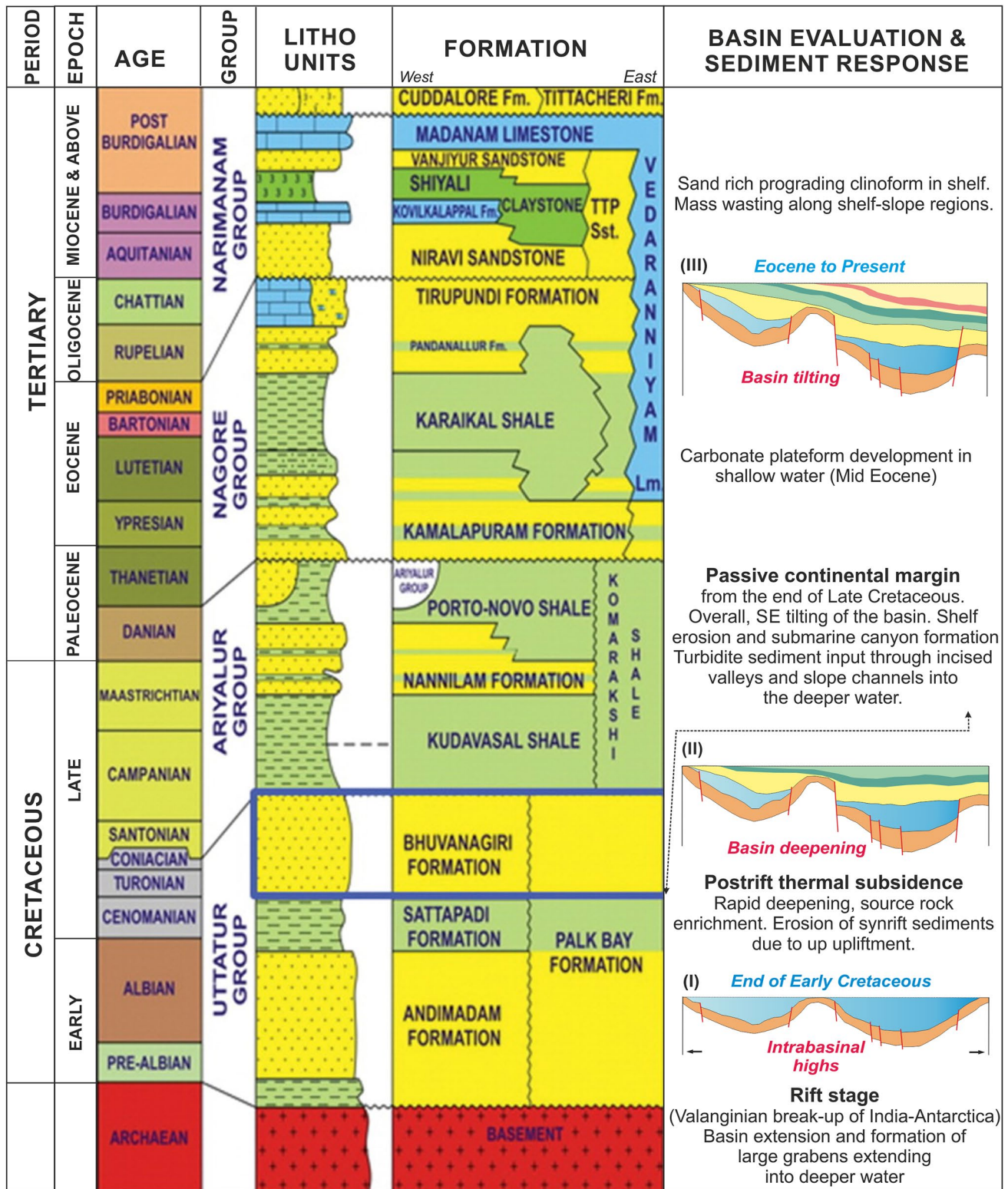


Fig. 2 Generalized stratigraphy of the Cauvery Basin. Different phases of basin evaluation, tectono-stratigraphic development, and associated sediment responses are also shown

environment due to rapid subsidence of the basin. These sediments indicate a relatively higher volume of sediment input from the surrounding granitic highs (Dubey and Mahapatra 2013). The Sattapadi shale formation (middle Karai shale in onshore) deposited in partly anoxic conditions largely consists of marine shales with occasionally thin-bedded silty calcareous sand and is considered to be an important source rock (2–2.5% of TOC) of the basin (Nagendra et al. 2011; Sain et al. 2014; Premarathne 2015; Bansal et al. 2019). The Sattapadi shale is conformably overlain by the sand-rich Bhuvanagiri Formation of the Cenomanian–Turonian age and the Kudavasal shale, a marine transgressive sequence, unconformably overlying to the Bhuvanagiri Formation (Fig. 2) (Nagendra et al. 2018; Chakraborty and Sarkar 2018; Sengupta et al. 2020).

The separation of Madagascar during the Cenomanian–Turonian period led to an overall SE tilting of the Cauvery-Palar Basins (Nagendra and Nallapa Reddy 2017). During the Turonian time, a distinct variable density channelized lobe (turbidite) system started prograding into the deeper water followed by deposition of transgressive shale. During this period, sedimentation in the basin took place under local and regional transgressive phases, represented by the Portonovo Shale and its equivalent, the Komarakshi Shale, which together attained a thickness of about 1000 m (Lasitha et al. 2019). Towards the western part of the

basin, the sand-rich Nannilam Formation of the Santonian–Campanian age provides significant exploration objectives (Chakravorti et al. 2006), which is unconformably overlain by thick Porto-Novo shale (top of Ariyalur group) of Campanian–Maastrichtian age. The Ariyalur–Pondicherry sub-basin in the northeastern part appears to have hosted the deep-water sedimentary facies during the Late Cretaceous (Paranjape et al. 2015). It was the period of widespread sedimentation under marine conditions of different local and regional transgressive phases. Towards the end of the Cretaceous, a major tectonic change took place in the basin, which began with the formation of an unconformity followed by an overall eastward tilting of the basin (Fig. 2) (Chakravorti et al. 2006; Lasitha et al. 2019). An interpreted regional seismic section of the deep-water Cauvery Basin is given in Fig. 3, which is showing fault-controlled basement architecture and a breakup unconformity (synrift top) (Misra and Dasgupta 2018). The distinct growth pattern of synrift and postrift sedimentary packages and downlapping reflection pattern over unconformity surface is clearly visible in this seismic section (Fig. 3). Overall, SE tilting of the basin during the end of the Late Cretaceous (Post Turonian) produced massive erosion of shelf-slope regions and deeply incised submarine canyons were developed (Susanth et al. 2021).

Consequently, siliciclastic sediments (turbidites) bypass the shelf-slope margins through deeply entrenched valleys,

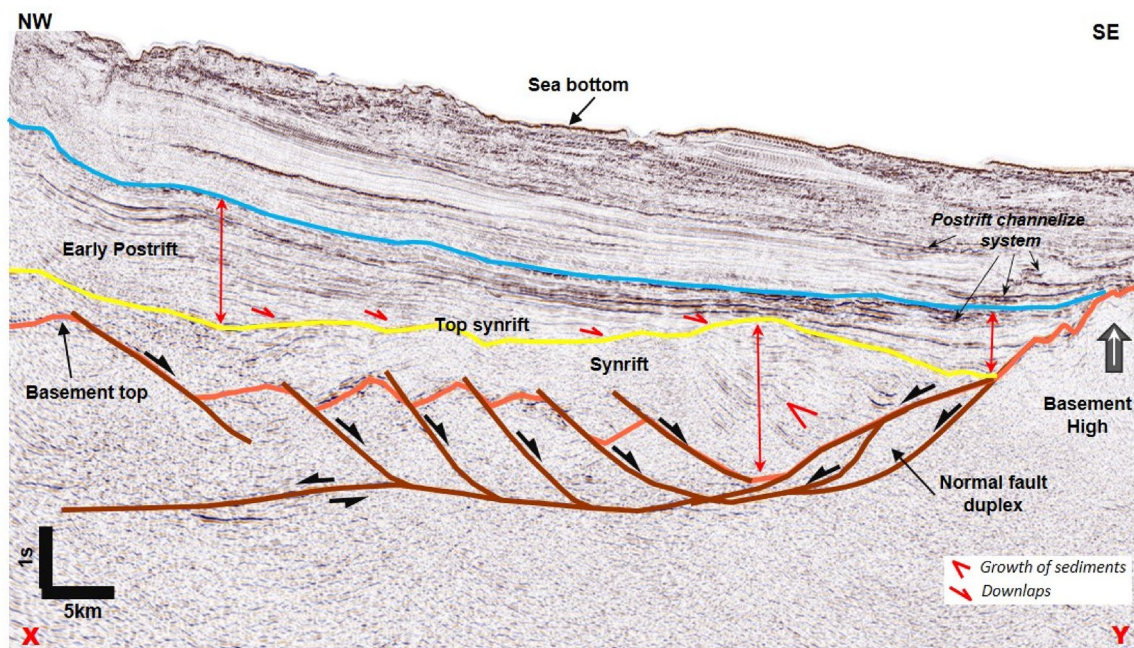


**Fig. 3** Interpreted regional Seismic section of deep-water Cauvery basin in NW–SE direction (location shown in Fig. 1b). The fault controlled basement architecture, rift geometry and a breakup unconformity (synrift top) are interpreted with regional scale seismic interpretation. The distinct growth pattern of sedimentary packages at synrift as well as postrift intervals, basinward progradation and down-

lapping geometry of early postrift reflectors over unconformity surface (due to post Cretaceous tilting) is clearly evident. Postrift channelized system (stacking pattern) is also interpreted based on bright amplitude cut and fill structures (modified after Misra and Dasgupta 2018).

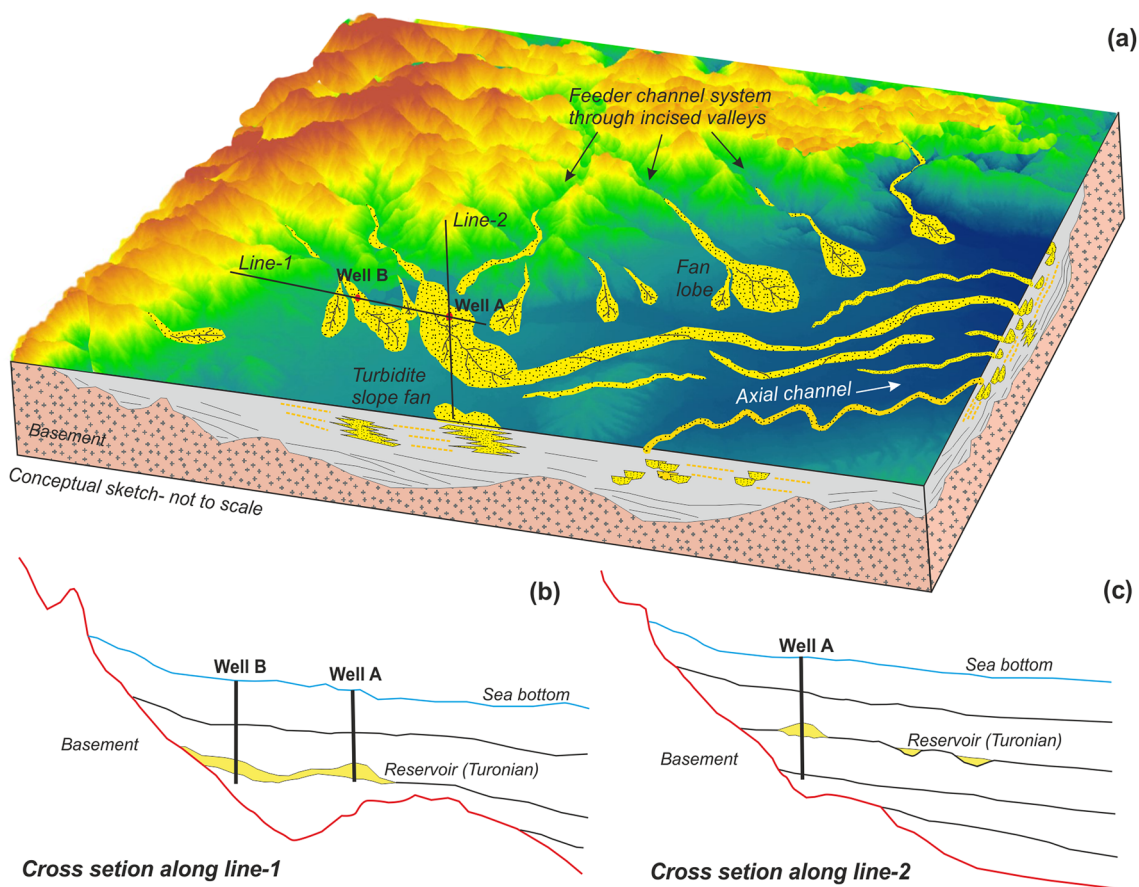


**Fig. 4** **a** A conceptual 3D sketch of the study area revealing the depositional pattern of the sandy turbidite channel fairways (shelf-slope feeder) and slope-fans through incised submarine canyons. The paleo-bathymetry controlled sediment input direction of feeder channels and depositional geometries of sedimentary facies (turbidites) is clearly shown in this sketch. **b** A subsurface cross-section connecting

through both the wells shows basement controlled stratigraphic architecture. Note that well B lies to the updip of discovery well A. **c** A subsurface cross-section through discovery well A, showing thickening of stratigraphy towards deeper water and development of turbidite reservoir at Turonian age

which leads to the development of turbidite slope fans and channelize fairways into the deeper water (Fig. 4). These turbidite sand fairways are the key postrift reservoirs of this basin. Subsequently, the tilting phase continued in the Tertiary period and prograding shelf-slope sequences were developed at a relatively faster pace (Muthuvairvasamy et al. 2003; Rao et al. 2010; Nagendra and Nallapa Reddy 2017). The later sections of this paper explain the geophysical characterization of Cenomanian–Turonian age reservoirs of two deep-water wells drilled in the offshore Cauvery Basin.

## Overview of the present study: a problem statement

In the present study, post-drill geophysical analysis was carried out for two exploratory wells (Well A & B), drilled in the northern part of the Cauvery Basin deep-water area by RIL at ~ 1200 m of water bathymetry (Fig. 5). Both these

drilled wells were lying in a similar geological set-up and were located within 5 km of the vicinity. The deep-water sediments of the late Cretaceous age were dominated by variable density turbidite channel-lobe sediments deposited typically in low sinuosity and relatively higher energy environments. The primary target of both wells was 30–40 m thick turbidite channel-lobe reservoir sands of the Turonian age. The pre-drill geological and geophysical investigation revealed that most of the attributes had an almost similar response and both the locations looked equally promising. The first exploratory well (well A) turned out to be a gas discovery (~ 35 m gross column), which improved the probability of reservoir presence and effectiveness at location B. The second well was proposed to establish the up-dip continuity of proven reservoir sands and to estimate the total hydrocarbon column thickness. Despite all the similarities between the two locations, the second well (well B) encountered diagenetically altered tight reservoir sands and hence was declared as a dry well. This well encountered high

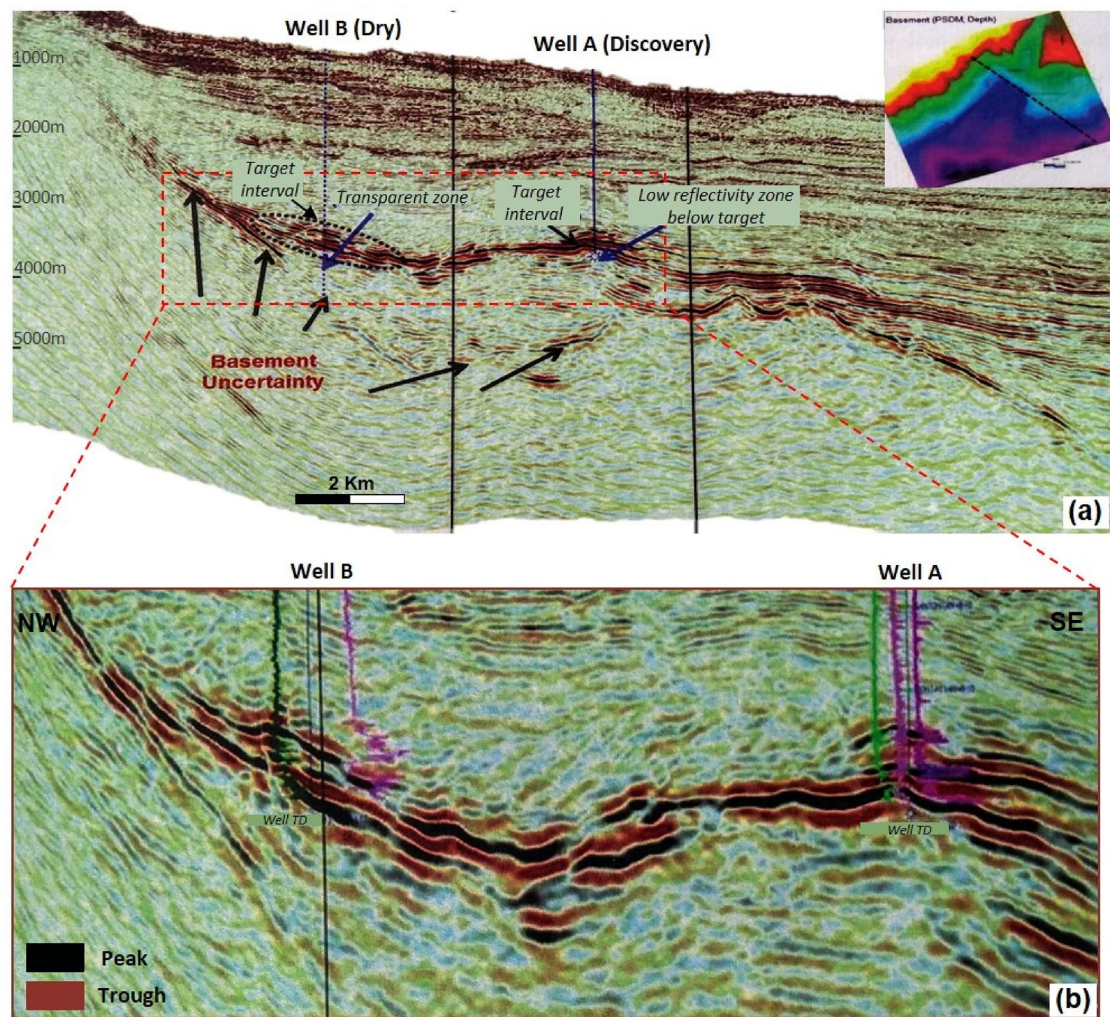


**Fig. 5** NW–SE trending Seismic sections of the study area located in the northern part of the Cauvery Basin. **a** An arbitrary seismic line connecting both the wells and showing regional setup, amplitude con-

trast and reflection continuity. **b** An enlarged seismic section at the target interval is overlain by Gamma and Resistivity logs at both the drilled well locations

impedance dry sands with minimal porosity and permeability. Post-drill petrophysical analysis of well B indicated the presence of basement-derived, short transported and poorly sorted sediments with poor porosity and permeability due to calcite cementation.

A systematic workflow was designed in the present study and multiple geophysical techniques were used for post-drill investigation of these twin wells (Figs. 5 and 6). Careful consideration was given to understanding the geological uncertainties and depositional heterogeneity of reservoirs by discriminating the geophysical properties using seismic attributes. A thorough investigation and comparison of pre-stack and post-stack seismic data of both the well locations indicated an effect of critical angle reflections in the seismic data in the reservoir interval. Typically, for the high impedance reservoirs having high P-wave velocity ( $V_p$ ) and high density, the critical angle

comes closer to around  $25^\circ$ – $30^\circ$ . These are the angles that are frequently used in stacking and for AVO studies (Zhang and Brown 2001; Russell 2014). The risk and uncertainty during prospect maturation increases, if the effect of critical angle reflection in the seismic amplitude analysis is not appropriately understood and taken into consideration. Offset synthetic modeling was performed which also pointed towards the effect of misleading far offsets. The current study demonstrates an excellent analog to compare the depositional heterogeneity of turbidite reservoirs and their geophysical characterization. This pre- and post-drill comparative analysis of geophysical data of two exploratory wells will be highly beneficial to readers and may help in de-risking the undrilled prospect inventory of a similar play type.

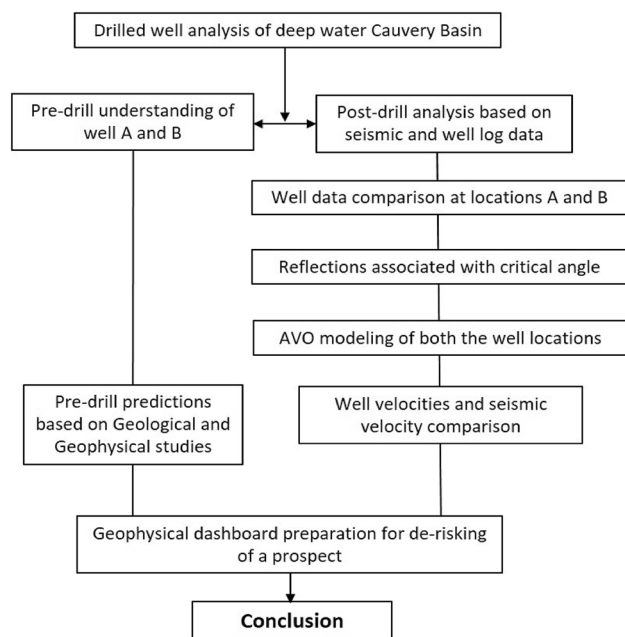


**Fig. 6** Flow chart showing the steps followed for post-drill Geophysical analysis of two drilled wells discussed in this paper

## Methodology and interpretation

This section explains the systematic workflow adopted for the pre and post-drill analysis of available geophysical data of both the drilled wells. The flow chart in Fig. 6 shows the step-wise process adopted during data analysis and geophysical dashboard preparation. The drilled well data, P-wave ( $V_p$ ) and S-wave ( $V_s$ ) velocities, density, Gamma, neutron density, and other logs were used for comparison and to recognize the differences in reservoir characteristics. Full-stack data, angle stacks (near angle stack 3–13°, mid angle stack 13–21°, far angle stack 21–27°), seismic attribute volumes and pre-stack time migrated (PSTM) as well as depth migrated (PSDM) gathers were analyzed in detail to understand the seismic waveform distortion from different perspectives like critical angle, multiples, stretching at far offsets, and interference due to bed thickness (Fig. 7). To understand the effect of variable lithology zero offset and full offset elastic synthetics were generated using log data. The objective was to demonstrate the effect of lithological changes in seismic once wavelets are introduced. The synthetics were generated and then compared with pre-SDM gathers at both the drilled locations to highlight the artifacts introduced by the seismic data acquisition and processing. Seismic interval velocities, an output of pre-stack depth migration were used along with sonic velocities to get an idea if seismic interval velocities were able to pick the reservoir variability or not. The handpicked tomographic velocities were found to be much closer to sonic velocities

compared to seismic interval velocities. Tomographic velocities were able to pick geological heterogeneity better than seismic interval velocities at the reservoir level.

### Pre-drill understanding of well A and B

The seismic amplitudes at both locations appeared to be equally bright (Figs. 5 and 7). The siliciclastic sediments encountered in both the wells at reservoir intervals were composed of moderate to coarse grain sands with mud matrix and fine streaks of calcareous sands. Generally, the well logs reveal calcite streaks locally, whereas the seismic perceives average properties over a much longer vertical scale. The synthetic seismogram generated at both locations revealed a strong amplitude at top of the reservoir compared to that in seismic (Fig. 7). The top part of the reservoir at well B encountered a layer of ~2.6 gm/cc density and velocities higher than 5 km/s. This layer was overlain by shale sequence and showed identical properties as that of brine reservoir sands overlying the shale section in well A. In such a situation the reflection coefficient corresponding to the target event at well B would be ~0.3 compared to ~0.12 at well A. This implies around 2.5 times increase in amplitude at well B with respect to well A, which was not evident in the seismic section traversing through both the wells. This explains why there was no gross increase in top sand amplitudes between A and B locations despite the significant difference in the subsurface lithology.

### Post Drill investigation of seismic and well data

For a better understanding of reservoir sands, a detailed post-drill analysis was taken up. Detailed AVO modeling was carried out to understand the behavior of seismic amplitudes at the two well locations. An attempt was made to understand the relation between the seismic amplitudes and the correlated facies encountered in the well. Prior to this, well seismic correlation was done using the well seismic tie method. Well to seismic tie was done using two softwares—Hampson Russel's ELOG and Landmark's Syntool. There was a very good match between Vertical Seismic Profiling (VSP), synthetics and the real seismic data. A good signal-to-noise ratio of around 4.5 was observed for both the wells in the data. There was an excellent match between synthetic and seismic with a strong event-to-event correlation, which boosted the confidence on how logs relate to seismic at both the well locations. In well A, the post-drill depth of the main objective (reservoir top) was only 2 m shallower than the prognosed depth whereas, in well B the post-drill depth of the main objective was shallower by ~125 m than the prognosed depth. The sands encountered in both the wells were



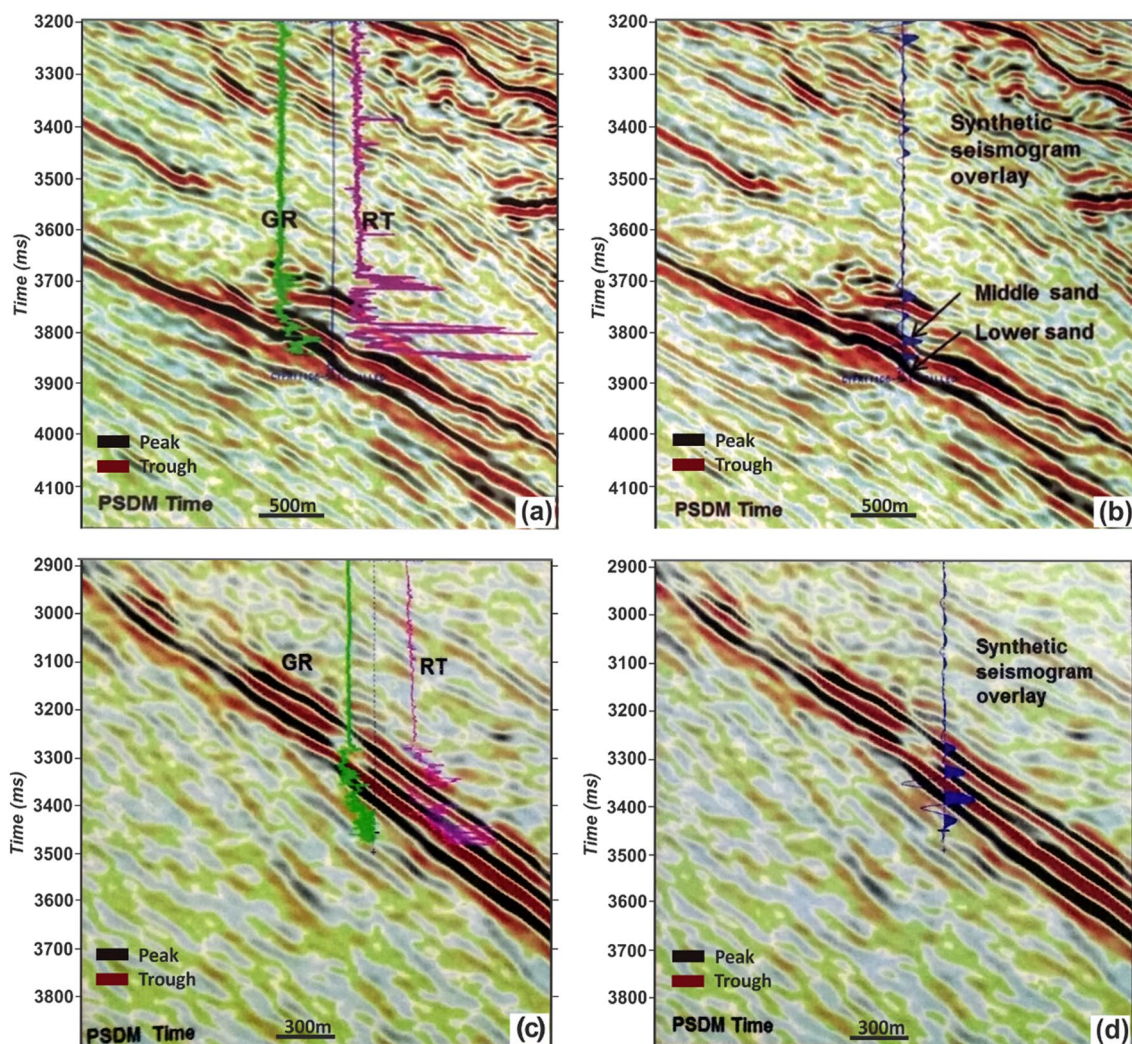


**Fig. 7** Comparative analysis of seismic data at both the wells. **a** Overlay of Gamma and Resistivity logs on the seismic section at discovery well A. **b** Synthetic seismogram overlay on the seismic section

at discovery well A. **c** Overlay of Gamma and Resistivity logs on the seismic section at dry well B. **d** Synthetic seismogram overlay on the seismic section at dry well B

high impedance sands and exhibited class 1 AVO in both datasets.

### Well data comparison at locations A and B

In well A, two sand intervals of 37 m (gas sand) and 54 m (11 m gas sand + 43 m brine sand) of Turonian age were encountered (Figs. 7 and 8). The 37 m gas sand had effective porosity in the range of 12–16%, clay content of 15% with an NTG ratio of 61%. The lower 11 m gas sand was of poor quality. It had only 6% effective porosity and ~50% clay content. The remaining 43 m brine sand was very good quality (NTG-93%). In well B, the prognosed reservoir interval appeared to have a high density ~2.6 gm/cc, implying the presence of tight calcite-rich rocks with velocities up to 5–6 km/s (Figs. 7 and 8). The sands encountered in well B

were diagenetically altered and had minimal effective porosity and no permeability. Possibly, the basement-derived and carbonate-rich sedimentation transported from adjacent updip areas contributed towards making up the reservoir encountered in well B.

The well logs from the two wells were plotted on top of each other for comparison of reservoir properties in the log domain (Fig. 9). Well A was given a shift of –100 m to match the sand interval in well B. Shales above the target reservoir in well B was 500 m/s faster than that in well A, whereas the shales within the reservoir had almost similar properties in both the wells. The first target in well B behaved like calcareous brine sand in well A. The reservoir interval at well B had high P wave velocities (~5–6 km/s) and densities in the range of 2.5–2.6 gm/cc, whereas in the case of the discovery well A, the P-wave velocities were

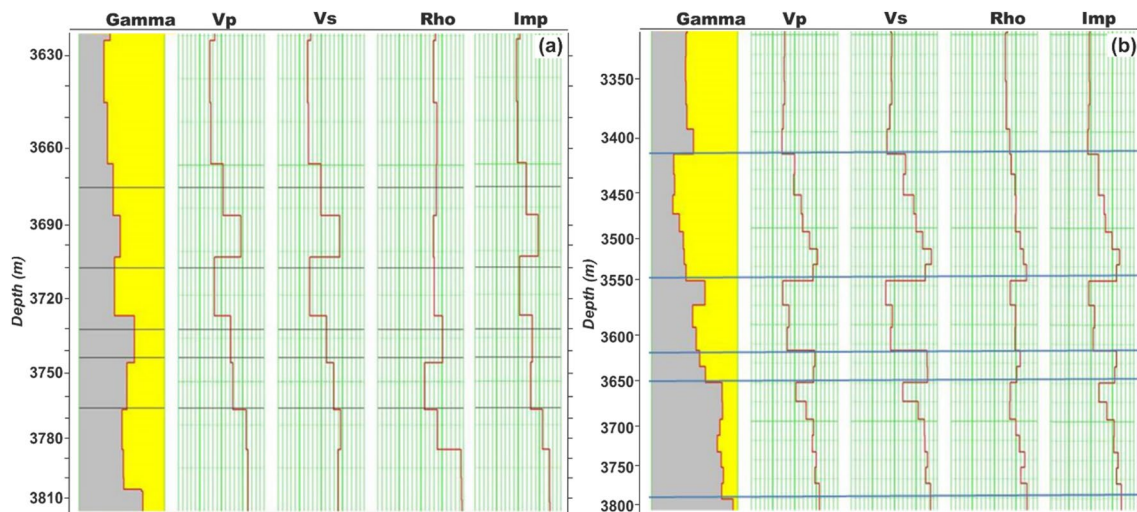


**Fig. 8** Display of post-drill logs (Gamma,  $V_p$ ,  $V_s$ , density and acoustic impedance) after blocking for both the drilled wells. **a** Discovery well A **b** Dry well B

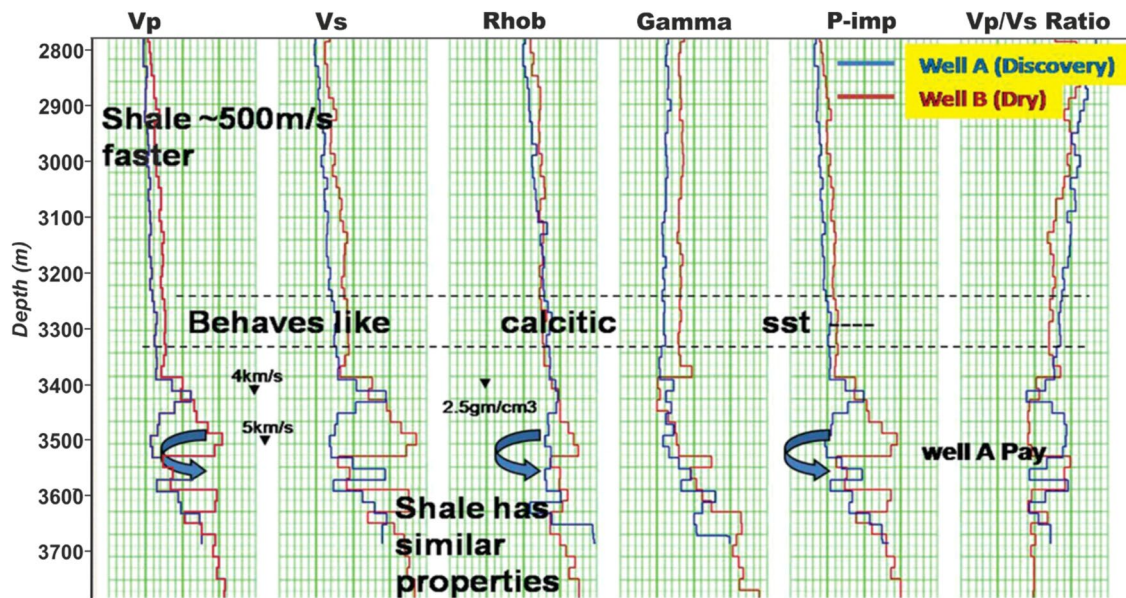


**Fig. 9** Log data ( $V_p$ ,  $V_s$ , Gamma, density, acoustic impedance and  $V_p/V_s$  ratio) overlay for both the wells (blue and red lines denote the discovery well A and dry well B respectively)

in the range of 3.5–4 km/s and densities in the range of 2.35–2.45 gm/cc. The porosity and permeability in the reservoir were destroyed due to calcite cementation for dry well B. Despite the presence of cement content in reservoir sands, the porosity and permeability were preserved for discovery well A.

The  $V_p/V_s$  ratio looks high for the discovery well (gas well) compared to the dry well indicating a high Poisson's

ratio (PR) in the discovery well and low PR in the dry well. Generally, Poisson's Ratio in gas saturated sand lies within 0–0.25 range, with typical value around 0.15. However, sometimes abnormally high PR values are observed in gas sand (Dvorkin 2006). Some well log measurements, persistently produce a Poisson's ratio as large as 0.3. This could be attributed to poor quality data or anisotropy. Other plausible explanations could be patchy saturation or sub-resolution thin layering. A cross-plot between the

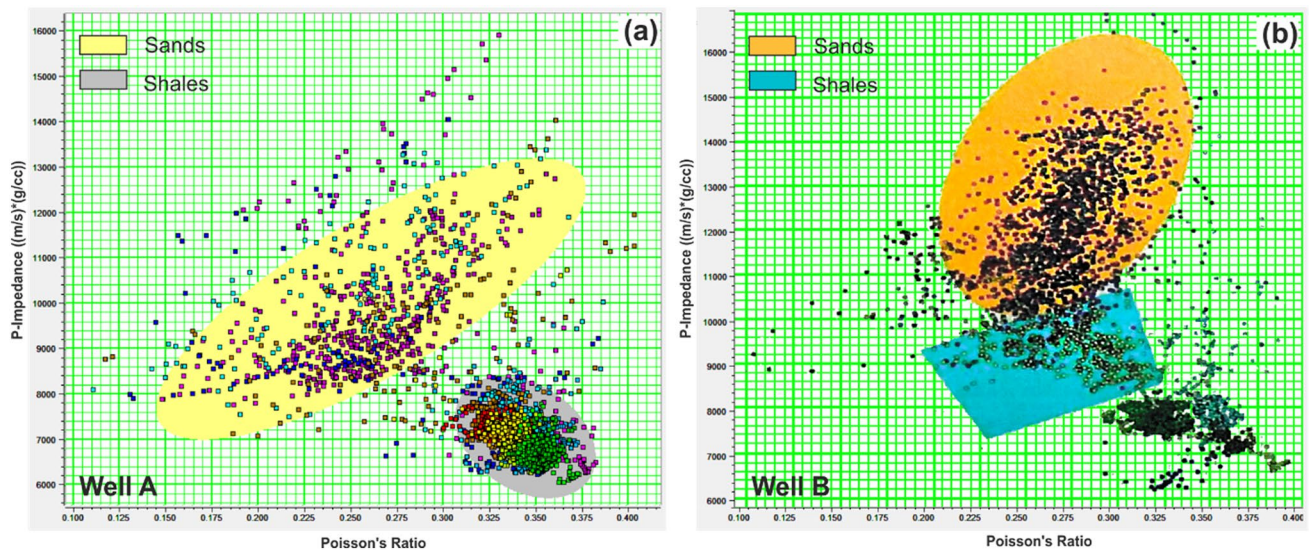


**Fig. 10** Acoustic impedance (AI) vs Poisson's ratio (PR) plot for well A (Discovery) and well B (Dry)

acoustic impedance (AI) vs Poisson's ratio (PR) for both the wells is shown in Fig. 10.

#### Direct Hydrocarbon Indicator and analysis of pre-stack gathers

While evaluating Direct Hydrocarbon Indicator (DHI) characteristics, an understanding of geological setting is crucial as an expected DHI response is dependent on it. The presence of a DHI in seismic data aids in de-risking of a prospect and has a significant impact on reserve calculation (Hilterman 2001; Roden et al. 2005, 2012; Hanafy et al. 2018). AVO analysis is a deterministic way to predict hydrocarbon presence from seismic data (Smith and Gidlow 1987; Rutherford and Williams 1989; Hilterman 1990; Castagna and Smith 1994; Smith and Sutherland 1996; Castagna et al. 1998; Figueiredo et al. 2019; Fawad et al. 2020). Before proceeding with AVO analysis, it is always good to do forward modeling of AVO responses based on geological setup, as a feasibility study. This is done by creating a synthetic seismic model based on an assumed or interpreted Earth model (Zeng et al. 2013). The synthetic seismic is then compared to the real seismic data, and if necessary, the Earth model can be edited to give a better match. AVO forward modeling can be used to analyze the variation of amplitude with offset. By assigning different  $V_p$ ,  $V_s$ , and densities according to different AVO classes, the response for various AVO classes can be regenerated by AVO forward modeling technique. More rigorous modeling could reveal the correct lithology (Roden et al. 2014). According to Break et al. 2006; Lasitha et al. 2019 in the pre-stack domain, the offset or angle is indicative of three important aspects of seismology. They are

(i) measuring the velocity of seismic waves in rocks, (ii) data redundancy (independent measurements of quantities that should be same-stacking offers the potential for signal enhancement by destructive interference of noise), (iii) procedures of migration which adds another element of complexity due to the presence of nonzero offsets.

Data in the pre-stack domain offers the possibility of identifying rocks by variation of reflection coefficients with offset or angle. With only zero-offset data, a little information can be deduced. However, with the full range of offsets at our disposal, a more thoughtful analysis can be tried. Reflection coefficients contain valuable information about the local medium properties on both sides of an interface. Therefore, analysis of amplitude variations with incidence angle or offset (AVA/AVO) is often used in reservoir characterization (Mallick and Frazer 1991; Avseth et al. 2001; Break et al. 2006; Ehirim and Chikezie 2017; Avseth and Lehocki 2021).

AVO analysis was carried out on the corresponding gathers at A and B well locations. A slight increase in amplitude from near to mid and then a drastic decrease in amplitude from mid to far (hump shape) was seen on PSTM as well as PSDM data at the reservoir level. To confirm that the hump shape seen in the behavior of reflection amplitudes in the PreSTM and PreSDM gathers was not a processing artifact, the Un-NMO'ed gathers were also analyzed. Similar AVO response (increase in amplitude from near to mid offset and then decrease in amplitude from mid to far offset) was observed in Un-NMO'ed gathers also. Although a similar response was seen for gathers at the B location and other leads and prospects in that area but the position of the hump with respect to offset could be used as a clue to de-risk other prospects post drilling of well B. AVO response was

observed to be more consistent in PSTM data where a consistent decrease in amplitude from near to far offset was seen which is indicative of class 1 high impedance gas sands. The AVO response was analyzed at neighborhood traces also and it was found to be in agreement with the above observations.

### Reflections associated with a critical angle

Many a time, the high impedance reservoirs are characterized by high contrasts in media parameters across the interface. This results in reflections associated with the critical reflections at relatively smaller offsets, where conventional AVO analysis is not valid anymore. For typical values of elastic properties, critical reflections occur at small angles of around 25°–30°. In general, 3°–35° is the range of angles frequently used in stacking and for AVO studies. If the angle range used for stacking and other AVO studies includes critical angle events, it may lead to false amplitudes in the stack data and mislead AVO analysis. Early emergence of critical angle indicates the presence of high velocity associated with an event corresponding to the identified prospect. (Makris and Thiessen 1984) have used critical reflections to image through high-velocity evaporite. The importance of near and post-critical reflections is highlighted by several researchers (Makris and Thiessen 1984; Vecken and Da Silva 2004; Downton and Ursenbach 2006; Skopintseva et al. 2012) who showed that using such reflections improves inversion results. Based on plane wave reflection coefficient analysis, (Hall and Kendall 2003; Landrø and Tsvankin 2006; Carcione and Picotti 2012), it is noticed that the critical angle is sensitive to the fracture orientation. The near and post-critical reflections generated by a point source, which are a function of the wavefront radius and frequency are explained by (Červený and Hron 1961; Alhussain et al. 2007). Recently developed spherical wave reflection coefficients for isotropic/anisotropic interfaces (Ayzenberg et al. 2007; Ursenbach et al. 2007) provide better insights into the reflection behavior observed around and beyond the critical angle. Analysis of the reflection coefficients for the isotropic interface shows that post-critical reflections contain information about the under-burden that cannot be recovered from pre-critical reflections. Pre-critical reflections have a higher sensitivity to P and S-wave velocities and anisotropy parameters (Lasitha et al. 2019).

The real gathers in the study were compared to check various aspects of pre-stack data at two locations (Fig. 11). The gathers were analyzed in detail to understand if seismic can capture those subtle differences that made two locations behave so differently. Far offsets in the real gathers were low in amplitude and post-critical effects were not seen clearly for location A. There was good near-to-far coherency. Mode conversions and inter-bed multiples were not prominent. Unlike location A, at location B the mode conversions

and inter-bed multiples were deforming the seismic image. Also, there was very poor near-to-far coherency. The critical distance, at which critical angle started emerging, was around 3200 m in well A and a small critical distance of only 2000 m was observed leading to a very early generation of critical angle effects at well B. Critical distance was calculated at both the wells for the interfaces having strong impedance contrast and it was observed that high-velocity contrast is responsible for shorter critical distances. The peak amplitudes for all three objectives were suddenly terminated into a trough, which can be easily confused with polarity reversal if not analyzed carefully.

Furthermore, the Critical angle was calculated using the formula  $\theta_c = \sin^{-1}(v_1/v_2)$  for both the offset synthetics using well velocities. The critical angle was found to be 36° for the discovery well and 34° for the dry well (Table 1). The observations made on these pre-stack gathers also indicated hard and fast lithology and thus some very strong reflection coefficients. Prominent refractions associated with the target event were seen in the pre-stack depth migrated gathers close to location B (Fig. 11).

### AVO modeling and synthetic seismogram generation

The modeling of acoustic responses (reflections associated with compressional waves and density) of stratigraphic features has become less common because of increased emphasis on the modeling of elastic responses (reflections associated with compressional waves, shear waves, and density). The use of P-wave velocity ( $V_p$ ), S-wave velocity ( $V_s$ ) and density provides an additional constraint on reservoir property predictions (Hart 2013).  $V_p$ ,  $V_s$  and density logs are used to generate the angle-dependent impedance log, which is further used for deriving reflectivity series. This reflectivity series is then convolved with a wavelet to generate a synthetic seismogram using algorithms such as Zoeppritz, Aki-Richards and a full-wave elastic modeling algorithm. The selection of the modeling algorithm depends on how the synthetics are going to be used. Aki-Richards approximation may give a better result than Zoeppritz for high contrast thin layers (Simmons and Backus 1994).

Hampson Russel Software (HRS) was used for AVO pre- and post-drill modeling studies. The two most important algorithms available for synthetic seismogram generation in HRS are, (i) Zoeppritz zero offset modeling algorithm and ii) full offset elastic modeling algorithm. The synthetic section was generated using Zoeppritz equations from a layered model. Rock properties ( $V_p$ ,  $V_s$ , and density) of different layers were used to model how much energy gets transmitted and gets reflected back at the interface. The amplitude of the reflected energy is calculated using Zoeppritz equations once the ray path for reflection from a boundary is determined. It is also possible to calculate P-wave and S-wave

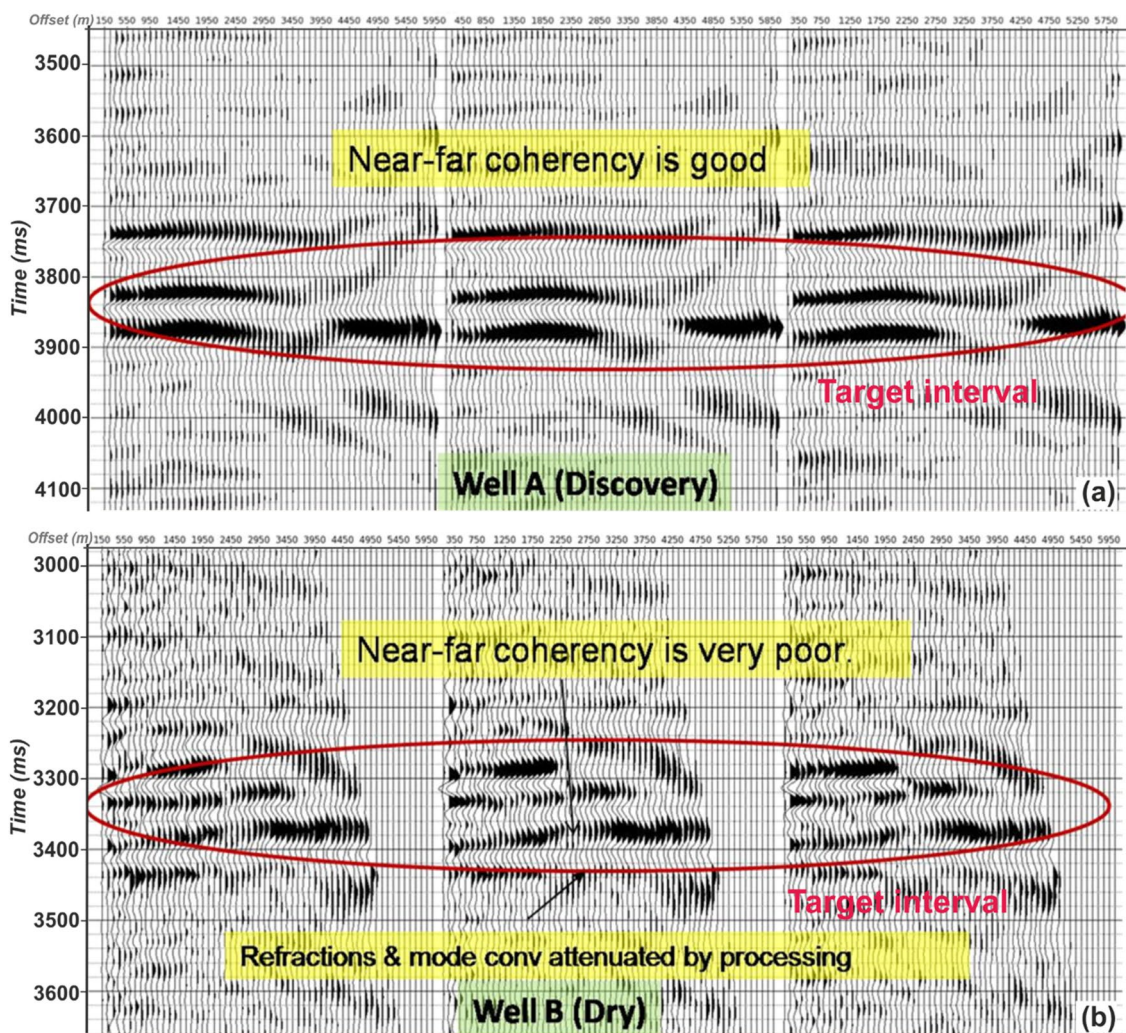


**Fig. 11** Comparative analysis of PSDM gathers of both the well locations. **a** PSDM gathers at discovery well A. **b** PSDM gathers at dry well B showing (Near-Far Coherency and Mode conversions)

**Table 1** Critical angle for the target events calculated using blocky log data

Well	Shale $V_p$ (m/s)	Sand $V_p$ (m/s)	$\theta_c$ ( $^\circ$ )
Discovery well A	3000	5100	36 $^\circ$
Dry well B	3236	5600	34 $^\circ$

reflection coefficients at different offsets using Zoeppritz equations. The conversion of P-wave to S-wave is also determined using these equations. When P-wave is incident on a plane reflector, it produces four resulting waves, P and S reflected waves and P and S transmitted waves. However, the Zoeppritz algorithm described above has some limitations. It uses ray tracing to determine the angle at which energy is incident on each surface. From knowledge of the incident angle and the lithological properties above and below

the interface, the reflection amplitude is calculated using Zoeppritz equations. While the Zoeppritz equation is strictly accurate for plane-wave energy incidents on a single interface, it does not model the reality where a spherical wave is incident on a collection of interfaces. This creates a series of inter-bed multiples and mode-converted waves. These waves may interfere with the primary reflections and change the resulting waveform. The Zoeppritz algorithm, because it models the primary energy only, may give an inaccurate result in that case, especially for thin-layer models for large impedance contrasts (Simmons and Backus 1994). Therefore, it is recommended to use the Elastic wave algorithm to generate synthetics for a better match with the acquired seismic data.

The elastic wave algorithm attempts to solve these problems by modeling all components simultaneously. It is designed to simulate the AVO effect of P wave reflectivity for

a model with complex reflection layering. As demonstrated by Simmons and Backus (1994), the mode conversions and multiples through those layers may affect the AVO response at the target level, and create P-wave reflections displaying an entirely different AVO response than those from the single elastic interface. For these reasons, the prestack seismic amplitude and the waveforms are recommended to be modeled using a full offset elastic wave modeling algorithm and a model with detailed stratigraphic layering should be used as input. This algorithm is theoretically exact for the one-dimensional case as it also models the multiples and mode-converted events. The most sophisticated modeling we have includes, transmission losses, geometrical spreading, mode conversions and internal multiples starting from well-sampled good quality well logs.

Transmission loss refers to the gradual loss of energy by the incident wavelet as it propagates through the series of layers above the target interface. Geometrical Spreading refers to the decrease in amplitude of the source wavelet as it propagates away from the source point (Ursin 1990). Real seismic data has usually been corrected during processing for geometrical spreading. Since the main purpose

of creating a synthetic is to compare it with real data, the effect can be overlooked while generating the synthetics. The synthetic seismograms generated are comparable with the seismogram that would be measured in the field. Often, it is desirable to compare the generated synthetics with real data that has been NMO corrected. For this reason, NMO-correction can be applied to synthetics while they are being generated. The process used for AVO modeling correctly models the real earth process, i.e. it produces a complete synthetic without NMO correction, and then applies NMO correction to that synthetic. This means that the true impact of NMO stretch can be seen on the generated synthetic.

### AVO modeling of both the well locations

The synthetic seismograms were generated at the two locations for comparison with the real gathers as well as for comparative analysis of the two synthetics to understand the missing link between the two prospects (Fig. 12). The seismic as expected seems to average out the details of the target zone captured in well data in both the wells. It is difficult to predict the results for well B if analyzed in isolation.

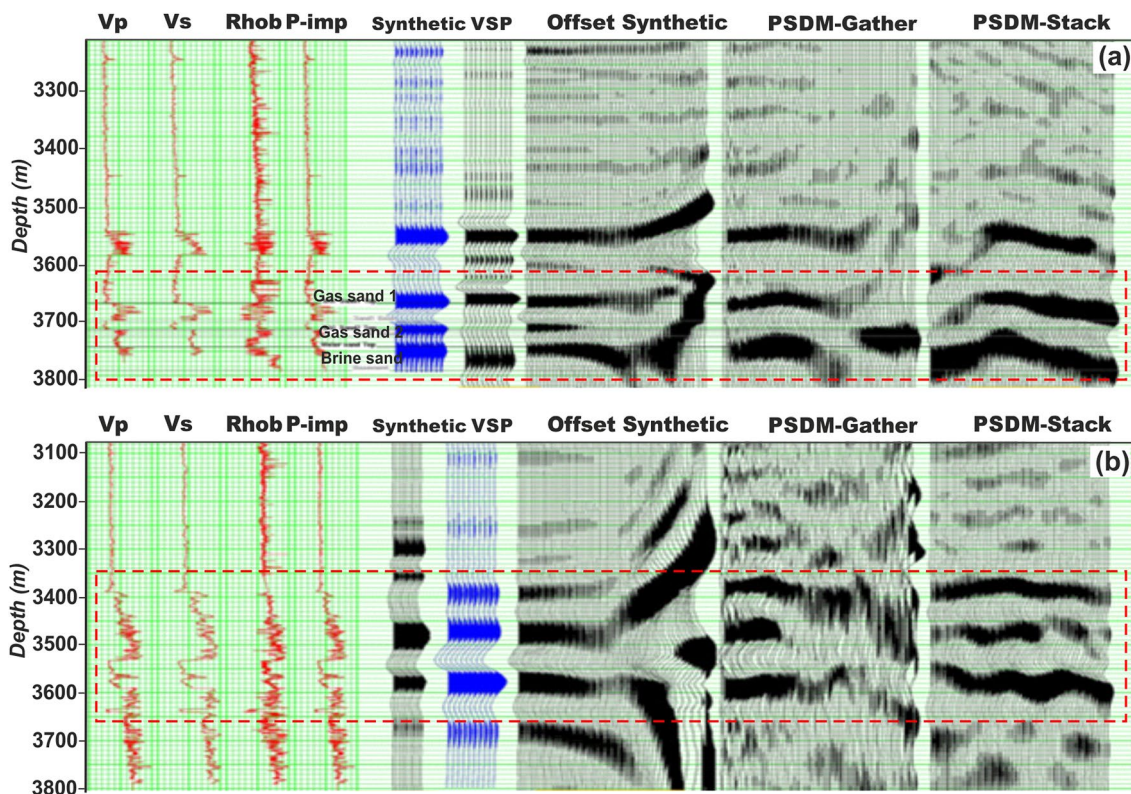


**Fig. 12** Synthetic modeling using in situ logs, and its comparison with VSP, PSDM gathers, and PSDM full-stack data. Red box denoting the area of interest. **a** Well logs, VSP, synthetic, PSDM gathers and PSDM stack data correlation of discovery Well A (left to right). Note the variation in resolved gas sands and brine sand in synthetics

is not picked up in seismic data. **b** At dry well B, synthetic as well as the gathers are showing very poor coherency between near-far offset events. Also, the internal multiples are attenuated in real gathers during the processing

However, the comparative analysis of the seismic observations at the two locations was enough to suggest that the two locations were different. For a better match with the real seismic data full offset elastic synthetics were generated. The intention was to understand how subsurface geology is responding and how events in the real seismic are correlating with the synthetics. Detailed understanding of various events in the offset domain and how they match in synthetic and seismic at the two locations could give a clue on reservoir properties across the reservoir at the well location.

Analyses of the synthetic gathers at two locations indicated Class 1 AVO response for the sands in the targeted zone, with strong reflections beyond critical offset and mode conversion effects at the far offset. The comparative study of offset synthetics modeled till 6 km with the real gathers at the well location was carried out. Beyond mid offset range, strong mode conversions and interbed multiples were also observed in synthetic seismograms at location B. This was not the case for well A. Though mode conversions and interbed multiples were seen for well A but they were not as evident as in synthetics for well B. Near to Far coherency was also very poor for location B when compared to that at location A. These mode conversions and internal multiples were not seen in real gathers as they were attenuated in processing. The observations in the pre-stack data like coherency, critical distance and abrupt termination of amplitudes were indicative of higher velocity sediments at location B.

The dotted yellow lines in Fig. 13 highlight unusually fast energy starting at a critical distance of 2 km. Distorted but apparently primary energy continuing to larger offsets suggested that the fast layer is not massive, but confined to a thin layer (behaving like a thick calcite streak). Critical distance (offset at which refraction overtakes reflection) may be used as another lithology diagnostic tool.

When incident angles are overlaid on synthetic offset gathers at two locations it was found that well B shows early emergence of critical angle effect and has distorted

the waveform at far offsets. Critical angle effects started at a lower angle at location B compared to that at well A suggesting strong velocity contrast for well B. Based on this analysis, it can be concluded that information regarding critical angle emergence gives a fair idea about velocity contrast in the subsurface. The pre-stack gathers, reflections pre and post-critical offset, should be observed and interpreted carefully while de-risking class I sands.

### Well velocities and seismic velocities at locations A and B

A conventional velocity analysis uses a collection of trial velocities. Each trial velocity is taken to be a constant function of depth and is used to flatten the data. Sometimes the events in the middle of the gather are nearly flattened, whereas the early events are under-corrected and later events are over-corrected. This is typical because the amount of move-out correction varies inversely with velocity, and the earth's velocity normally increases with depth. A measure of the goodness of fit of the NMO velocity to the earth velocity is found by summing the CDP gathers over the offset. Presumably, the better the velocities match, the better (bigger) will be the sum and the better is the signal-to-noise ratio (S/N). The process is repeated for many velocities, and the best sum is picked up for the final NMO correction.

The same process was followed during conventional velocity analysis and NMO application while processing seismic data. During post-drill analysis of two wells, location-specific velocity analysis was carried out and tomographic velocities were generated as an output at both locations (Fig. 14). These tomographic velocities in addition to migration velocities were analyzed in detail and it was found that location B tends to have tomographic velocities approximately 200 m/s faster than at location A, which couldn't be picked up by the migration velocities because of its regional nature (Fig. 14). The sediments having densities of 2.6 gm/cc and velocities of 5–6 km/s in the reservoir at location B

**Fig. 13** Enlarged section of the PSDM gathers at the Dry well location highlighted by a red box in Fig. 12b. Note the change of character at ~2 km offset



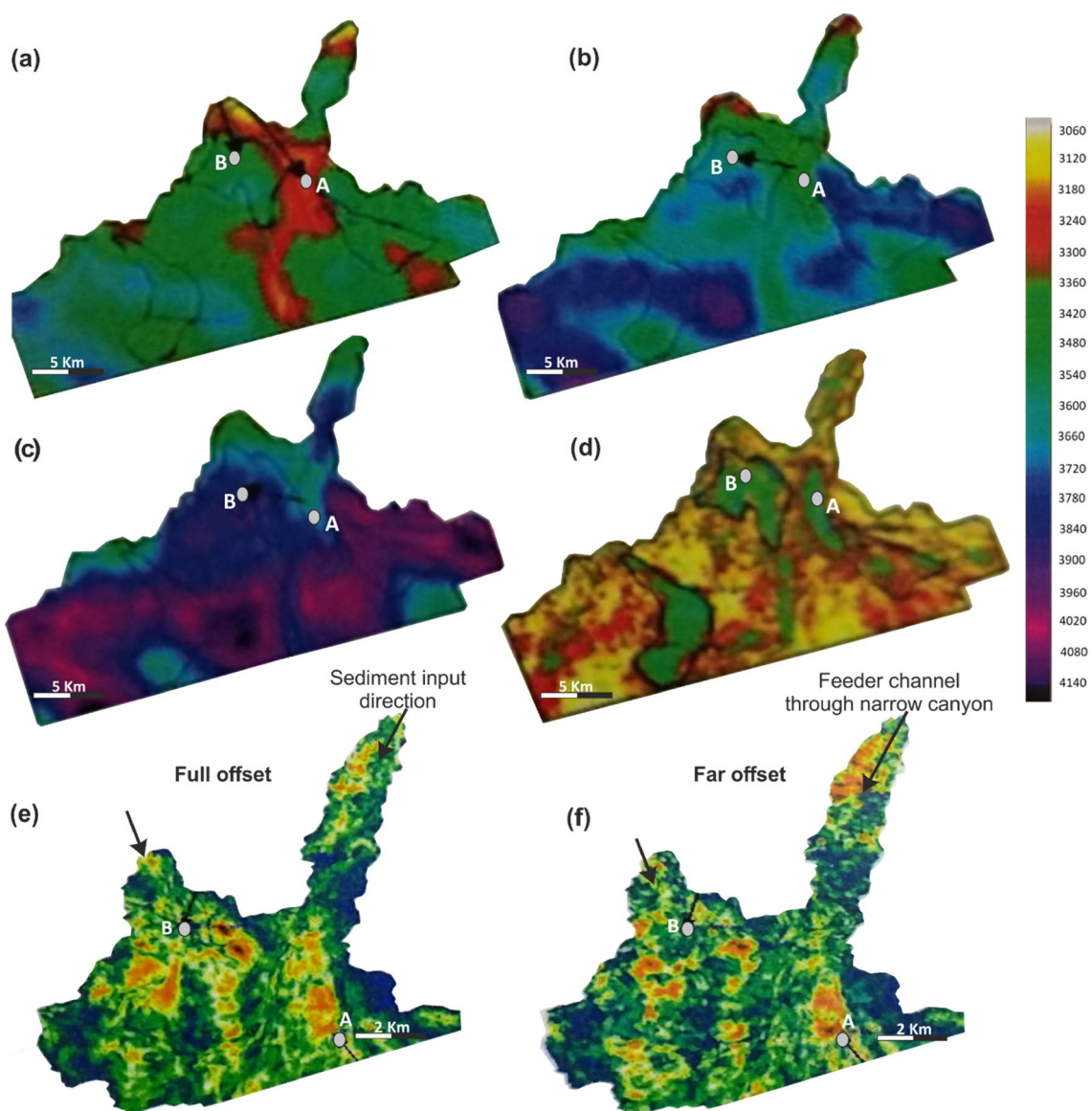


**Fig. 14** Tomographic velocity slices and amplitude maps around both the well locations. **a** Velocity slice at the reservoir interval. It is noticed that location B tends to have approximately 200 m/s faster velocities than that at location A. **b** Velocity slice above 200 ms from the target interval. **c** Velocity slice below 200 ms from the target interval showing variation at both the locations. **d** RMS amplitude

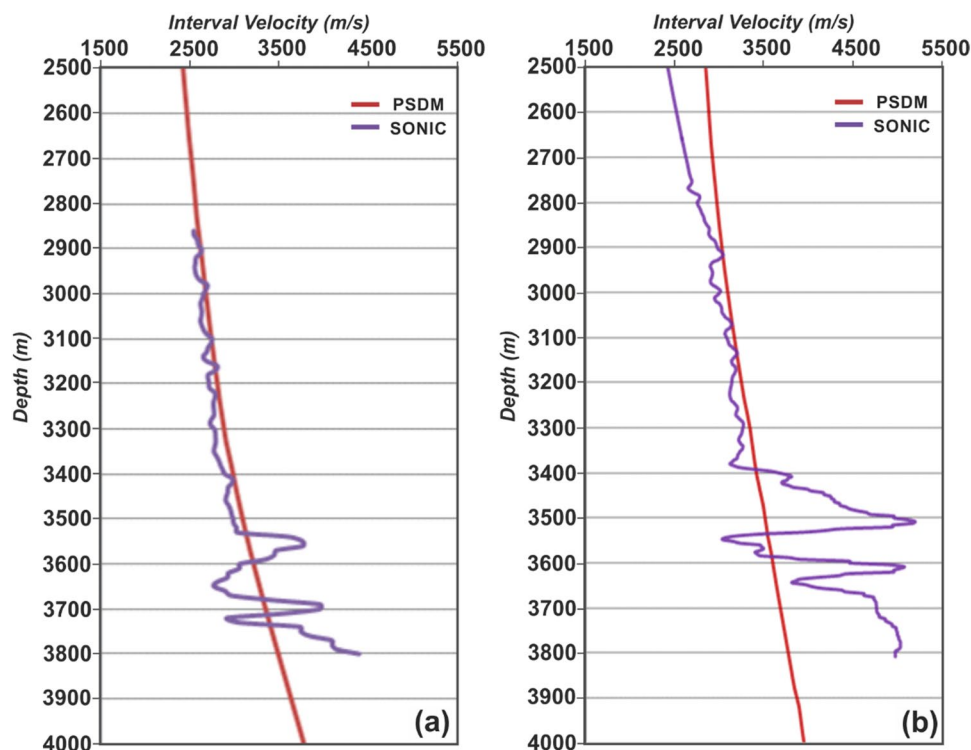
map at the reservoir interval showing channelized lobe geometry. **e** Maximum positive amplitude with 40 ms window around both the wells on full offset data showing sediment input direction. **f** Maximum positive amplitude with 40 ms window around both the wells on far offset data. Note the feeder channel feeding the sediments at well A location through a narrow canyon appears to bypass location B

seems not to be deposited by the feeder channel feeding the sediments at well A and appear to bypass the location B. It is evident that velocities give indirect evidence regarding the presence of lithology type in the subsurface, but it is not always possible to pick the sharp velocity changes using seismic velocities. The combination of near offset amplitudes and interval velocities at the thick sediment entry point may help in distinguishing calcareous sediments from clean sands.

The seismic interval velocities were also compared with the well velocities, to analyze the predrill velocity behavior (Fig. 15). The comparison of seismic velocities and well velocities at locations A and B showed a low-velocity trend in seismic at the reservoir level, compared to the trend in the well velocities. Location B encountered much faster velocities post drill, which was not picked up by seismic prior to drilling. This fast velocity nature at location B was very well evident in gathers at the target level but was somehow overlooked in the light of positive results at location



**Fig. 15** Seismic interval velocity (red curve) comparison with sonic velocity (purple curve) for both the wells. **a** Discovery well A. **b** Dry well B



A. Reflections beyond the critical offset as discussed above were much more prominent at location B as compared to location A. The comparison showed that the background velocity at B was higher than that at A. The top 20 m sand interval has similar reservoir properties at both locations. Velocities at location B became faster at the deeper level as the sands had no porosity due to calcite cementation and the presence of basement-derived material. There are issues with PSDM gather flattening/processing. However, the best data available in hand and the best technology available in the company suggested different observations at two locations. It is observed that careful analysis of gathers may provide useful information in terms of reservoir properties, especially in class 1 high impedance sand. Advanced techniques like FWI may enhance resolution to some extent.

### Discussion: a dashboard for de-risking of a prospect

Analyzing minor details of seismic data like critical and post-critical reflections, seismic velocities, and gather behavior at far offsets may give a reasonable idea regarding reservoir quality and its hydrocarbon potential. The observed seismic signatures in full-stack and partial stacks and pre-stack gathers hide useful information associated with reservoirs. Class 1 sand is usually associated with high velocities (Fawad et al. 2020). These higher velocities sometimes lead to critical and post-critical reflections in the recorded offset

range. Multiple reflections and mode conversions along with an early generation of critical angle reflection from the top and bottom of the reservoir may make AVO analysis troublesome. The early generation of critical angle many a time appears to show a faster drop in amplitude as observed in Class 1 gas sands, which is in general considered to be a DHI for high impedance sands. The present study reveals a detailed analysis of all the available information and integrated interpretation along with an understanding of data in the pre-stack domain which may indicate the presence of high-velocity formations. The attributes like refraction velocity, critical distance, and coherency between events in the near and far offsets play an important role in the identification of lithology at the reservoir level. Also, Pre-stack depth migration velocities give a fair idea of what could we expect beneath the reservoir. Careful analysis and understanding of gather behavior at the far offsets may indicate high-velocity formations.

In addition to all the above attributes, forward modeling plays a major role in characterizing reservoirs. Forward modeling integrated with detailed analysis and interpretation of all the observations made on the seismic data has the power to save a well as demonstrated. The clarity of the critical angle and its role in deforming the observed seismic signature is highlighted in this study using forward modeling. The velocities often act as a good indicator of lithology and hence reservoir quality and therefore should be analyzed in detail while maturing a prospect. A comparison of seismic interval velocities with the sonic velocities revealed that

**Fig. 16** Geophysical dashboard comprising the list of minor observations that may be used to de-risk a reservoir in terms of reservoir quality

Attributes	Observations at Well A	Observations at Well B
Refractions Xcritical	Large	Short
Refraction Velocity	Slow	High
Coherency (Near-Far)	Good	Poor
Amps vs Background	Average	Extreme
Handpicked Vint	Slower	Faster
Tomographic Velocity	Slower	Faster
Mode Conversions/Internal Multiples	Minor	Strong
AVO (including AI/GI study)	2, 2p	1 (or none)

seismic tomography was not able to model fast velocities encountered in dry well B. The role of far offset information in identifying strong post-critical offset effects due to the presence of high-velocity sediments has been demonstrated well using AVO forward modeling.

Based on the above study, a checklist was prepared for the qualitative de-risking of prospects (Fig. 16). This checklist gives a direct tool to scrutinize prospects apart from other studies. It has very well distinguished the two prospects which otherwise looked equally promising. The observations at location B, the dry well, are indirectly pointing towards high velocity diagenetically altered poor quality reservoirs. The checklist proposed here will help in reducing the uncertainty in characterizing a reservoir and its deliverability in addition to a better understanding of the seismic signatures. The subtle differences in the geophysics of the two locations identified before drilling could have saved a dry well. The thoughtful analysis of waveform distortions, by studying the pre-stack gathers, will increase the interpreter's predictability regarding reservoir properties. Forward modeling gives the interpreters a strong handle to play with and identify reservoir extremities by varying the rock properties (Hart and Chen 2004).

## Conclusions

1. The current study demonstrates that it is possible to distinguish between softer/slower/possibly better reservoir rocks (Well A) and hard/fast/tight reservoir rocks (Well B) lying in a deep-water environment by carefully examining various aspects of seismic data (seismic events, amplitudes, frequency) and their association with sub-surface stratigraphy.

2. The seismic amplitude strength both within and outside the reservoir, critical and post-critical reflections, seismic velocities, and gather behavior at large offsets can give a fair idea of the type/quality of the reservoir and its hydrocarbon potential.
3. Though it is difficult to zero down the uncertainties associated with the prospect using forward seismic modeling, it has the potential to mitigate the risk associated with any prospect.
4. The integration of regional tectono-geological setup with basin level Gross Depositional Environment (GDE) maps of sediment fairway distribution and their linkage with high-quality 3D seismic analysis can play a significant role in reservoir forecasting and qualitative interpretation of prospects in the inventory.
5. The proposed geophysical dashboard may help to reduce the risk of drilling a dry well and provide greater confidence to the interpreter when predicting reservoir properties and its deliverability if used in conjunction with the geological depositional model.

**Acknowledgements** The authors gratefully acknowledge Reliance Industries Limited, India for allowing this academic research work. Part of this paper is a doctoral research work of Minakshi Mishra.

**Author's contribution** MM contributed to conceptualization, methodology, software, and geophysical data analysis and interpretation. AKP contributed to conceptualization, geological studies, seismic data interpretation, sediment deposition analysis, and software. Finally, both the authors concluded the outcomes, wrote, reviewed, and edited this paper.

**Funding** This research is not funded by any specific grant from funding agencies in the public, commercial, or not-for-profit sectors.

## Declarations

**Conflict of interest** Both the authors declare that there is no conflict of interest in the publication of this paper.

**Open Access** This article is licensed under a Creative Commons Attribution 4.0 International License, which permits use, sharing, adaptation, distribution and reproduction in any medium or format, as long as you give appropriate credit to the original author(s) and the source, provide a link to the Creative Commons licence, and indicate if changes were made. The images or other third party material in this article are included in the article's Creative Commons licence, unless indicated otherwise in a credit line to the material. If material is not included in the article's Creative Commons licence and your intended use is not permitted by statutory regulation or exceeds the permitted use, you will need to obtain permission directly from the copyright holder. To view a copy of this licence, visit <http://creativecommons.org/licenses/by/4.0/>.

## References

- Allhussain M, Gurevich B, Urosevic M (2007) Experimental verification of spherical wave effect on the AVO response and implications for three-term inversion. In: SEG Technical Program Expanded Abstracts. pp 249–253
- Avseth P, Lehocki I (2021) 3D Subsurface modeling of multi-scenario rock property and AVO feasibility cubes—an integrated workflow. *Front Earth Sci* 9:160. <https://doi.org/10.3389/feart.2021.642363>
- Avseth P, Mukerji T, Jørstad A et al (2001) Seismic reservoir mapping from 3-D AVO in a North Sea turbidite system. *Geophysics* 66:1157–1176. <https://doi.org/10.1190/1.1487063>
- Ayzenberg MA, Aizenberg AM, Helle HB et al (2007) 3D diffraction modeling of singly scattered acoustic wavefields based on the combination of surface integral propagators and transmission operators. *Geophysics* 72. <https://doi.org/10.1190/1.2757616>
- Bansal U, Pande K, Banerjee S et al (2019) The timing of oceanic anoxic events in the Cretaceous succession of Cauvery Basin: constraints from 40 Ar/39 Ar ages of glauconite in the Karai Shale Formation. *Geol J* 54:308–315. <https://doi.org/10.1002/gj.3177>
- Bastia R, Radhakrishna M, Srinivas T et al (2010) Structural and tectonic interpretation of geophysical data along the Eastern Continental Margin of India with special reference to the deep water petroliferous basins. *J Asian Earth Sci* 39:608–619. <https://doi.org/10.1016/j.jseaes.2010.04.031>
- Biswas SK, Bhasin AL and, Jokhan R (1993) Classification of Indian sedimentary basins in the framework of plate tectonics. In: Biswas SK, Alak D, Garg P, Pandey J, Maithani A, Thomas NJ (eds) Proceedings of the second seminar on petroliferous basins of India. Indian Petroleum Publishers, Dehradun, pp 1–46
- Break F, Veeken P, Rauch-davies M (2006) KMS Technologies—KJT Enterprises Inc. Publication AVO attribute analysis and seismic reservoir characterization AVO attribute analysis and seismic reservoir characterization, pp. 41–52
- Carcione JM, Picotti S (2012) Reflection and transmission coefficients of a fracture in transversely isotropic media. *Stud Geophys Geod* 56:307–322. <https://doi.org/10.1007/s11200-011-9034-4>
- Castagna JP, Smith SW (1994) Comparison of AVO indicators: a modeling study. *Geophysics* 59:1849–1855. <https://doi.org/10.1190/1.1443572>
- Castagna JP, Swan HW, Foster DJ (1998) Framework for AVO gradient and intercept interpretation. *Geophysics* 63:948–956. <https://doi.org/10.1190/1.1444406>
- Červený V, Hron F (1961) Reflection coefficients for spherical waves. *Stud Geophys Geod* 5:122–132. <https://doi.org/10.1007/BF02585356>
- Chakraborty N, Sarkar S (2018) Syn-sedimentary tectonics and facies analysis in a rift setting: Cretaceous Dalmiapuram Formation, Cauvery Basin, SE India. *J Palaeogeogr* 7:146–167. <https://doi.org/10.1016/j.jop.2018.02.002>
- Chakravorti C, Chandra S, Rana MS, et al (2006) Mapping of sub-aqueous canyon and channel fill reservoirs of Kamalapuram formation: a new exploration target in Ramnad Sub basin, Cauvery Basin, pp 963–968
- Chand S, Subrahmanyam C (2001) Gravity and isostasy along a sheared margin—Cauvery basin, Eastern Continental Margin of India. *Geophys Res Lett* 28:2273–2276
- Chetty TRK, Rao YJB (2006) Strain pattern and deformational history in the eastern part of the Cauvery shear zone, southern India. *J Asian Earth Sci* 28:46–54. <https://doi.org/10.1016/j.jseaes.2005.05.010>
- da Silva Pimentel Figueiredo K, SP, Temoteo KW, Gonçalves RX et al (2019) AVO Didactic analysis from simplified modeling of seismic data in libra oil field of the pre-salt region, Brazil. *Oalib* 06:1–14. <https://doi.org/10.4236/oalib.1105788>
- Dasgupta S (2019) Implication of transfer zones in rift fault propagation: Example from cauvery basin. *Indian East Coast Springer Geol*, pp 313–326. [https://doi.org/10.1007/978-3-319-99341-6\\_10](https://doi.org/10.1007/978-3-319-99341-6_10)
- Downton JE, Ursenbach C (2006) Linearized amplitude variation with offset (AVO) inversion with supercritical angles. *Geophysics*, 71. <https://doi.org/10.1190/1.2227617>
- Dubey S, Mahapatra M (2013) Understanding the deep syn-rift petroleum systems of Cauvery Basin: a 2D case study from Ramnad Basin. In: 10th Biennial International Conference & Exposition, pp 1–6
- Dvorkin J (2006) Can gas sand have a large Poisson's ratio? *SEG Tech Progr Expand Abstr* 25:1908–1912. <https://doi.org/10.1190/1.2369900>
- Ehirim CN, Chikezie NO (2017) Anisotropic avo analysis for reservoir characterization in Derby Field Southeastern Niger Delta. *IOSR J Appl Phys* 09:67–73. <https://doi.org/10.9790/4861-0901016773>
- Fawad M, Hansen JA, Mondol NH (2020) Seismic-fluid detection—a review. *Earth Sci Rev* 210:103347. <https://doi.org/10.1016/j.earscirev.2020.103347>
- Hall SA, Kendall JM (2003) Fracture characterization at Valhall: application of P-wave amplitude variation with offset and azimuth (AVOA) analysis to a 3D ocean-bottom data set. *Geophysics* 68:1150–1160. <https://doi.org/10.1190/1.1598107>
- Hanafy S, Farhood K, Mahmoud SE et al (2018) Geological and geophysical analyses of the different reasons for DHI failure case in the Nile Delta Pliocene section. *J Pet Explor Prod Technol* 8:969–981. <https://doi.org/10.1007/s13202-018-0445-4>
- Hart B, Chen M (2004) Understanding seismic attributes through forward modeling. *Lead Edge (Tulsa, OK)* 23:834–841
- Hart BS (2013) Whither seismic stratigraphy? *Interpretation* 1:SA3–SA20. <https://doi.org/10.1190/INT-2013-0049.1>
- Hilterman F (1990) Is AVO the seismic signature of lithology? A case history of Ship Shoal-South Addition. *Lead Edge* 9:15–22. <https://doi.org/10.1190/1.1439744>
- Hilterman FJ (2001) Seismic amplitude interpretation. Society of exploration geophysicists and European Association of Geoscientists and Engineers
- Janardhanan M, Goswami BG, Prasad J (2013) Petroleum source rock evaluation of the argillaceous sediments in a part of Nagapattinam Sub basin, Cauvery Basin. In" 10th Bienn Int Conf Exhib Soc Pet Geophys, pp 1–5
- Lal NKKK, Siawal A, Kaul AKKK, Lal NK, Siawal AK (2009) Evolution of East Coast of India—a plate tectonic reconstruction. *J Geol Soc India* 73:249–260

- Landrø M, Tsvankin I (2006) Seismic critical-angle reflectometry: a method to characterize azimuthal anisotropy? *SEG Tech Progr Expand Abstr* 25:120–124. <https://doi.org/10.1190/1.2369736>
- Lasitha S, Twinkle D, John Kurian P et al (2019) Geological features, hydrocarbon accumulation and deep water potential of East Indian basins. *Mar Pet Geol* 13:731–744. <https://doi.org/10.1016/j.jseaeas.2019.103981>
- Makris J, Thiessen J (1984) Wide-angle reflections: a tool to penetrate horizons with high acoustic impedance. *Contrasts*. In: 1984 SEG Annual Meeting, SEG 1984. Society of Exploration Geophysicists, pp 672–674
- Mallick S, Frazer LN (1991) Reflection/transmission coefficients and azimuthal anisotropy in marine seismic studies. *Geophys J Int* 105:241–252. <https://doi.org/10.1111/j.1365-246X.1991.tb03459.x>
- Mazumder S, Tep B, Pangtey K, Mitra D (2019) Basement tectonics and shear zones in Cauvery Basin (India): implications in hydrocarbon exploration, pp 279–311
- Mishra M, Singh KH (2019) Unravelling an anomalous seismic response using seismic modelling: a case study from Cauvery Basin, offshore East Coast India. *First Break* 37:35–41. <https://doi.org/10.3997/1365-2397.2019015>
- Misra AA, Dasgupta S (2018) Shallow detachment along a transform margin in Cauvery Basin, India. In: Misra AA, Mukherjee S (eds) *Atlas of structural geological interpretation from seismic images*. Wiley, New York, pp 101–105
- Muthuvairvasamy R, Stüben D, Berner Z (2003) Lithostratigraphy, depositional history and sea level changes of the Cauvery Basin, southern India. *Geol Anal Balk Poluostrova* 65:1–27. <https://doi.org/10.2298/gabp0301001m>
- Nagendra R, Nallapa Reddy A (2017) Major geologic events of the Cauvery Basin, India and their correlation with global signatures - a review. *J Palaeogeogr* 6:69–83. <https://doi.org/10.1016/j.jop.2016.09.002>
- Nagendra R, Kamalak Kannan BV, Sen G et al (2011) Sequence surfaces and paleobathymetric trends in Albian to Maastrichtian sediments of Ariyalur area, Cauvery Basin, India. *Mar Pet Geol* 28:895–905. <https://doi.org/10.1016/j.marpetgeo.2010.04.002>
- Nagendra R, Sathiyamoorthy P, Pattanayak S et al (2013) Stratigraphy and paleobathymetric interpretation of the Cretaceous Karai shale formation of Uttatur Group, TamilNadu, India. *Stratigr Geol Correl* 21:675–688. <https://doi.org/10.1134/S0869593813070046>
- Nagendra R, Reddy AN, Jaiprakash BC et al (2018) Integrated Cretaceous stratigraphy of the Cauvery Basin, South India. *Stratigraphy* 15:245–249. <https://doi.org/10.29041/strat.15.4.245-259>
- Narasimha Chari MV, Sahu JN, Banerjee B et al (1995) Evolution of the Cauvery basin, India from subsidence modelling. *Mar Pet Geol* 12:667–675. [https://doi.org/10.1016/0264-8172\(95\)98091-1](https://doi.org/10.1016/0264-8172(95)98091-1)
- Nemčok M, Sinha ST, Stuart CJ et al (2013) East indian margin evolution and crustal architecture: Integration of deep reflection seismic interpretation and gravity modelling. *Geol Soc Spec Publ* 369:477–496. <https://doi.org/10.1144/SP369.6>
- Nemčok M, Rybár S, Sinha ST et al (2016) Transform margins: development, controls and petroleum systems—an introduction. *Geol Soc Spec Publ* 431:1–38. <https://doi.org/10.1144/SP431.15>
- Paranjape AR, Kulkarni KG, Kale AS (2015) Sea level changes in the upper Aptian-lower/middle(?) Turonian sequence of Cauvery Basin, India—an ichnological perspective. *Cretac Res* 56:702–715. <https://doi.org/10.1016/j.cretres.2014.11.005>
- Premarathne U (2015) Petroleum potential of the Cauvery Basin, Sri Lanka: a review. *J Geol Soc Sri Lanka* 17:41–52
- Qin Y, Zhang G, Ji Z et al (2017) Geological features, hydrocarbon accumulation and deep water potential of East Indian basins. *Pet Explor Dev* 44:731–744. [https://doi.org/10.1016/S1876-3804\(17\)30084-8](https://doi.org/10.1016/S1876-3804(17)30084-8)
- Rao M V, Chidambaram L, Bharktya D, Janardhanan M (2010) Integrated analysis of late Albian to middle Miocene sediments in Gulf of Mannar Shallow Waters of the Cauvery Basin, India: a sequence stratigraphic approach. In: 8th Bienn Int Conf Explor Pet Geophys, pps 1–9
- Rigzone (2007) Reliance makes deepwater gas discovery in the Cauvery Basin | Rigzone. In: *Oil Gas News*. [https://www.rigzone.com/news/oil\\_gas/a/47798/reliance\\_makes\\_deepwater\\_gas\\_discovery\\_in\\_the\\_cauvery\\_basin/](https://www.rigzone.com/news/oil_gas/a/47798/reliance_makes_deepwater_gas_discovery_in_the_cauvery_basin/). Accessed 12 April 2021
- Rigzone (2013) Reliance, BP Discover gas condensate in Cauvery Basin | Rigzone. In: *Oil Gas News*. [https://www.rigzone.com/news/oil\\_gas/a/128616/reliance\\_bp\\_discover\\_gas\\_condensate\\_in\\_cauvery\\_basin/](https://www.rigzone.com/news/oil_gas/a/128616/reliance_bp_discover_gas_condensate_in_cauvery_basin/). Accessed 12 April 2021
- Roden R, Forrest M, Holeywell R (2012) Relating seismic interpretation to reserve/resource calculations: insights from a DHI consortium. *Lead Edge* 31:1066–1074. <https://doi.org/10.1190/tle31091066.1>
- Roden R, Forrest M, Holeywell R (2005) The impact of seismic amplitudes on prospect risk analysis. *Soc Explor Geophys—75th SEG Int Expo Annu Meet SEG 2005* 794–797. <https://doi.org/10.1190/1.2148278>
- Roden R, Forrest M, Holeywell R et al (2014) The role of AVO in prospect risk assessment. *Interpretation* 2:SC61–SC76. <https://doi.org/10.1190/INT-2013-0114.1>
- Russell BH (2014) Prestack seismic amplitude analysis: an integrated overview. *Interpretation* 2:SC19–SC36. <https://doi.org/10.1190/INT-2013-0122.1>
- Rutherford SR, Williams RH (1989) Amplitude-versus-offset variations in gas sands. *Geophysics* 54:680–688. <https://doi.org/10.1190/1.1442696>
- Sain K, Rai M, Sen MK (2014) A review on shale gas prospect in Indian sedimentary basins. *J Indian Geophys Union* 18:183–194
- Saravanan PS, Johnny A (2018) Study of Cambay and Krishna-Godavari Basin for shale oil and gas. *Int J Innovative Res Sci Technol* 4:63–72
- Sastri VV, Sinha RN, Gurcharan S, Murti KVS (1973) Stratigraphy and tectonics of sedimentary basins on East Coast of Peninsular India. *Am Assoc Pet Geol Bull* 57:655–678
- Sastri VV, Venkatachala BS, Narayanan V (1981) The evolution of the east coast of India. *Palaeogeogr Palaeoclimatol Palaeoecol* 36:23–54. [https://doi.org/10.1016/0031-0182\(81\)90047-X](https://doi.org/10.1016/0031-0182(81)90047-X)
- Sengupta SS, Singh J, Prakash R, Harilal (2020) Reservoir facies mapping, depositional environment, and implication for hydrocarbon occurrence: a case study from Ariyalur-Pondicherry sub-basin, Cauvery Basin, India. *Lead Edge* 39:909–917. <https://doi.org/10.1190/tle39120909.1>
- Simmons JL, Backus MM (1994) AVO modeling and the locally converted shear wave. *Geophysics* 59:1237–1248. <https://doi.org/10.1190/1.1443681>
- Skopintseva L, Aizenberg A, Ayzenberg M et al (2012) The effect of interface curvature on AVO inversion of near-critical and postcritical PP-reflections. *Geophysics*, 77. <https://doi.org/10.1190/geo2011-0298.1>
- Smith GC, Gidlow PM (1987) Weighted stacking for rock property estimation and detection of gas. *Geophys Prospect* 35:993–1014. <https://doi.org/10.1111/j.1365-2478.1987.tb00856.x>
- Smith GC, Sutherland RA (1996) The fluid factor as an AVO indicator. *Geophysics* 61:1425–1428. <https://doi.org/10.1190/1.1444067>
- Susanth S, Kurian PJ, Bijesh CM et al (2021) Controls on the evolution of submarine canyons in steep continental slopes: geomorphological insights from Palar Basin, southeastern margin of India. *Geo-Marine Lett* 41(41):1–27. <https://doi.org/10.1007/S00367-021-00685-9>

- Twinkle D, Srinivasa Rao G, Radhakrishna M et al (2016) Crustal structure and rift tectonics across the cauvery–palar basin, eastern continental margin of india based on seismic and potential field modelling. *J Earth Syst Sci* 125:329–342. <https://doi.org/10.1007/s12040-016-0669-y>
- Ursenbach C, Haase A, Downton J (2007) Efficient spherical-wave AVO modeling lead edge. *Geol Geophys* 26:1584–1589. <https://doi.org/10.1190/1.2821946>
- Ursin B (1990) Offset-dependent geometrical spreading in a layered medium. *Geophysics* 55:492–496. <https://doi.org/10.1190/1.1442860>
- Vecken PCH, Da Silva M (2004) Seismic inversion methods and some of their constraints. *First Break* 22:47–70. <https://doi.org/10.3997/1365-2397.2004011>
- Watkinson MP, Hart MB, Joshi A (2007) Cretaceous tectonostratigraphy and the development of the Cauvery Basin, south-east India. *Pet Geosci* 13:181–191. <https://doi.org/10.1144/1354-079307-747>
- Zeng H, Hart BS, Wood LJ (2013) Introduction to special section: interpreting stratigraphy from geophysical data. *Interpretation* 1:SA1–SA2. <https://doi.org/10.1190/INT2013-0614-SPSEIN.1>
- Zhang H, Brown RJ (2001) A review of AVO analysis. *CREWES Res Rep* 13:357–380
- Zhang G, Qu H, Chen G et al (2019) Giant discoveries of oil and gas fields in global deepwaters in the past 40 years and the prospect of exploration. *J Nat Gas Geosci* 4:1–28. <https://doi.org/10.1016/j.jnggs.2019.03.002>

**Publisher's Note** Springer Nature remains neutral with regard to jurisdictional claims in published maps and institutional affiliations.